The Notch1/Delta-like-4 axis is crucial for the initiation and progression of oral squamous cell carcinoma

Christian T. Meisel[1], Riccardo Destefani[1], Ilaria J. Valookkaran[1], Aashil Batavia[2], Niels Rupp[2], Cristina Porcheri[1]* and Thimios A. Mitsiadis[1]*

[1] Institute of Oral Biology, Faculty of Medicine, University of Zurich, Plattenstrasse 11, 8032 Zurich, Switzerland

[2] Department of Pathology and Molecular Pathology, University Hospital Zurich, Rämistrasse 100, 8091 Zurich, Switzerland

* Correspondence: thimios.mitsiadis@zzm.uzh.ch and cristina.porcheri@zzm.uzh.ch

Abstract

The Notch signaling pathway is frequently altered in oral squamous cell carcinoma (OSCC), the most common malignant neoplasm of the oral mucosa. This study aimed to elucidate the functional role of this pathway in both the initiation and progression of OSCC. Using transgenic animal models, advanced imaging, and next-generation-sequencing techniques, we analyzed Notch-dependent changes driving OSCC. We found specific expression patterns of Notch1 and Delta-like-4 confined to the malignant tissue, while Jagged1 was downregulated in OSCC. This mutually exclusive expression of Delta-like-4 and Jagged1 occurs at the early hyperplastic stage and persists until more advanced stages of the developing tumor. Transcriptomic analyses confirmed the dysregulation of the Notch pathway circuitry and of the genes associated with the undifferentiated state of OSCC cells. Furthermore, pharmacological Notch inhibition significantly impaired cancer cell motility. Taken together, these results reveal the pivotal importance of the Notch1/Delta-like-4 signaling axis as a central oncogenic driver in OSCC.

Keywords

Notch signaling pathway, oral cancers, squamous cell carcinoma, OSCC, transgenic mice, keratinocyte differentiation, Notch inhibitors, Notch ligands, Delta-like-4, Notch1, Jagged1, Notch1 Cre mice.

List of abbreviations

4NQO	– 4-nitroquinoline-1-oxide
CSL	– CBF, Suppressor of Hairless, Lag-1
Dll4	– Delta-like-4
DMSO	– Dimethyl sulfoxide
E-Cad	– E-cadherin
EMT	– Epithelial-to-mesenchymal-transition
GFP	– Green fluorescent protein
GO	– Gene Ontology
GSEA	– Gene set enrichment analysis
Hes	– Hairy and enhancer of split-1
Hey	– Hairy and enhancer of split related with YPRW motif protein
HNSCC	– Head and neck squamous cell carcinoma
Jag1	– Jagged1
K5/10/14	– Keratin 5/10/14
MesoSPIM	– Mesoscale selective plane illumination microscopy
OSCC	– Oral squamous cell carcinoma
RBPj	– Recombining binding protein suppressor of hairless
Runx1	– Runt-related transcription factor 1
Sox2	– SRY-Box Transcription Factor 2
TAM	– Tamoxifen

Main

Head and neck squamous cell carcinoma (HNSCC) is the sixth most common type of cancer, annually affecting 850.000 people worldwide [1–3]. Although modern multimodal therapy has improved clinical management of this disease, tumor recurrence and distal metastasis correlate with a poor prognosis, with a median overall survival of ten months [4,5]. HNSCC regroups a variety of cancers arising from the oral mucosa, nasal cavities, pharynx, and larynx, which have their own unique carcinogenic evolution and clinical score [6]. Oral squamous cell carcinoma (OSCC) originates from the mucosa of the oral cavity and develops progressively, starting with local hyperplasia of squamous epithelial cells and advancing through dysplastic and invasive stages [7,3]. In squamous dysplasia, clusters of proliferative, non-keratinized, poorly differentiated cells form an outgrowth on the epithelial surface (papillary carcinoma) [8]. Aberrant epithelial cells may infiltrate the neighboring muscles and spread along the mesenchymal lines to metastasize to cervical lymph nodes [4,8]. Proximal metastases occur in up to 50% of patients and are associated with the recurrence and development of distant metastases [6,9,10]. OSCC onset often relates to chronic exposure to genotoxic compounds, which in turn leads to genetic instability and the dysregulation of the DNA repair process [7]. Clones with acquired genetic alterations have an initial growth advantage and can potentially transform into aggressive subclones in the more advanced stages of the disease [11,12,13]. High-risk premalignant lesions can be subtle, and timely recognition relies on the detection of stage-specific molecular biomarkers.

Mutational profiling consistently identified chromosomal alterations resulting in the amplification of *cyclin D1* and EGFR regions, while genetic mutations affecting tongue epithelium have been mapped in cyclin-dependent kinase inhibitor 2A (CDKN2A), tumor protein 53 (TP53) [3,14,15], and the Notch signaling pathway, one of the major mutation hotspots in

OSCC [16–18]. Notch signaling is an evolutionary conserved pathway involved in cell fate specification and differentiation [19]. Epithelial functionality is supported by Notch signaling, especially in tissues and organs of the oral cavity, where it governs epithelial development and homeostasis since the earliest stages of embryogenesis [19–24]. In mammals, four Notch receptors (Notch1-4) and five Notch-ligands (Jagged1,2 and Delta-like-1,3,4) have been identified [25,26]. Upon receptor-ligand binding, a series of cleavages take place to ultimately release the Notch intracellular domain (NICD), which then translocates into the nucleus and acts as a transcription factor in a complex with CSL (also known as RBPj) [19,27]. The spatial distribution of each specific receptor, ligand, and their corresponding downstream targets reflects distinct functions that influence tissue physiology and homeostasis [28]. Dysregulation of Notch signaling is found in several human pathologies, and novel therapeutic approaches have been developed in recent years to specifically target Notch components [28,29]. Although genetic screenings have identified the Notch signaling pathway as one of the most commonly mutated pathways in OSCC[16–18], the precise role of Notch in the initiation and development of this malignancy remains largely unknown, with contrasting results that are supportive of either an oncogenic or a tumor-suppressive role [30–34].

In this study, we have first investigated the functional role of Notch signaling in OSCC using transgenic animal models. We found that the mutually exclusive expression of Dll4 and Jag1 is maintained in all stages of tumor growth, from initiation to the most advanced aggressive stages. Further, transcriptome analyses confirmed the *in vivo* studies and identified dysregulation of genes associated with the differentiation process. Finally, human cancer cell behavior was greatly affected by Notch specific blockage. Collectively, our data highlight the importance of

the Notch1-Dll4 signaling axis in OSCC initiation and progression, identifying a promising target for the treatment of this malignancy.

Materials and Methods

Animals

C57Bl/6 and *Notch1*^{CreERT}*:R26mTmG*$^{fl/fl}$ mice were used for this study [35,36],The mice were maintained and handled according to the Swiss Animal Welfare Law. This study was approved by the Cantonal Veterinary office, Zurich (License ZH197/2017 and ZH086/2021).

4NQO treatment of mice – OSCC murine model

For the induction of OSCC, treated mice received drinking water containing 50µg/mL 4NQO (#N8141, Sigma-Aldrich) starting at week 6 until week 22 of age. Control mice were littermates receiving drinking water containing the same volume of DMSO (#D4540, Sigma-Aldrich). The drinking solution was renewed twice a week. Females and males were equally represented in the experimental set-up. After 16 weeks mice were either euthanized (time point 22 weeks) or given normal drinking water until euthanasia (time point 32 weeks or 38 weeks). For lineage tracing Notch1-driven expression, Cre was activated by the intraperitoneal injection of tamoxifen 50mg/kg dissolved in corn oil/10% EtOH (Sigma-Aldrich Cat#T5648) for two consecutive days. All analyses were conducted in groups of 3 to 5 mice ($n \geq 3$).

Sample embedding and cryo-sectioning

After tissue isolation, samples were post fixed in 4% Paraformaldehyde (PFA) for 1h at 4°C and cryopreserved in 30% sucrose. Tissues were embedded in a cryo-embedding matrix (Tissue-Tek, O.C.T Compound, Sakura) and stored at -80°C until sectioning. Samples were sectioned (10µm) in the cryostat (Leica CM3050S) and stored at -80°C until staining.

Hematoxylin & Eosin staining

Sections were washed for 3x5min in 1x PBS. Nuclei were stained with Hematoxylin for 20 seconds (Sigma-Aldrich #51275). Cytoplasm was then stained with Eosin for 10 seconds (Sigma-Aldrich #HT110216), thoroughly washed and mounted for imaging. Images were acquired using the Leica DMC5400 microscope.

Immunostaining of cryosections

Immunofluorescence staining of cryosections was performed as previously described[37]. Used primary antibodies: polyclonal rabbit anti-Keratin14 (1:100; Poly19053, Biolegend), polyclonal goat anti-E-Cadherin (1:200, AF748, R&D Systems), polyclonal goat anti-GFP (1:100; ab6673; Abcam), polyclonal rabbit anti-DLL4 (1:100; ab7280; Abcam), polyclonal goat anti-DLL4 (1:50; AF1389; R&D) polyclonal rabbit anti-Jag1 (1:100; ab7771; Abcam), polyclonal rabbit anti-Keratin10 (1:100; PRB-159P; Biolegend), polyclonal Rabbit anti-Keratin5 (dilution 1:100; ab64081; Abcam) polyclonal rabbit anti-Notch1 (D1E11) (dilution 1:100; 3608S; Cell Signaling), polyclonal rabbit anti-Runx1 (dilution 1:100; HPA004176; Atlas Antibodies), polyclonal rabbit anti-p63 (dilution 1:100; ab53039; Abcam), monoclonal rabbit anti-Vimentin (dilution 1:100; ab92547; Abcam), mouse anti-Snail (1:100, #14-9859-80 Invitrogen). Used secondary antibodies: Goat anti-Rabbit IgG 488, Alexa Fluor Plus 488 (dilution 1:1000; A32731, Invitrogen), goat anti-mouse IgG 647, Alexa Fluor Plus 647 (dilution 1:1000; A32728, Invitrogen), donkey anti-Goat IgG 488, Alexa Fluor Plus 488 (dilution 1:1000; A32814; Invitrogen); donkey anti-Rabbit IgG 647, Alexa Fluor 647 (dilution 1:1000; A32795: Invitrogen), streptavidin Alexa Fluor 488 (dilution 1:100; S11223; Invitrogen). Nuclear

counterstaining was performed using DAPI (4',6-Diamidino-2-Phenylindole, Dihydrochloride, #D1306, Invitrogen).

Image acquisition – Confocal microscopy

Immunofluorescence images of the tongue tissue were produced using a Leica DM6000B microscope or Confocal Leica SP5/ SP8 with the following settings: 1024x1024 pixel dimension; 400Hz laser; frame average 3 or 4. photomultipliers PMT or Hyd. Fluorochromes used: Alexa 488, 546, 594, 647. A range of 10μm (standard) to 70μm (whole mount) thick Z-stack was analyzed collecting images every 2μm (standard) or 10μm (whole mount). Images were processed using Imaris 9.9 software (Bitplane). Photomerge Script from Photoshop (Adobe, Version 23.0.2) was used for overview images reconstruction.

Tissue clearance

The separated epithelial sheet was embedded in 2% low-melting agarose. The tissue was then transferred into Histodenz (#D2158, Sigma-Aldrich), dissolved in PBS1X and diluted until a measurable refractive index of 1.457 for tissue clearance.

Whole-organ 3D imaging

Whole tongue images were recorded with a custom-made selective plane illumination microscope (mesoSPIM) [39]. SPIM imaging was done after clearing and refractive index matching. The laser/filter combinations for mesoSPIM imaging were as follows: for Notch1-GFP at 488 nm excitation, a 405-488-561-640 nm QuadrupleBlock bandpass filter was used as the emission filter; for membrane localized dt-Tomato at 561 nm excitation, a 561 nm long pass filter was used. Transparent tongue epithelial whole-mount was imaged at a voxel size of 3.26 ×

3.26 × 3 µm (X × Y × Z). Further technical details of the mesoSPIM have been previously reported [39] (*mesoSPIM.org*).

Enzymatic separation of keratinized epithelium from mesenchyme of the murine tongue

Separation was performed as previously described [38]. In brief, an enzymatic cocktail of collagenase A (1mg/mL; Roche) and Dispase II (2mg/mL; #D4693 Sigma-Aldrich;) in 0.1 M PBS1X was injected into the subepithelial space from the posterior cutting end of the tongue. Upon incubation at 37°C for 30 min the mesenchyme and epithelium were pulled in opposing directions until complete separation is achieved.

RNA isolation epithelial tissue

Separated epithelial sheets were snap-frozen with liquid nitrogen and homogenized on ice for 3min using a motor driven grinder (Pellet Pestle Motor, Kontes). Further isolation according to manufacturer's instructions (RNeasy Mini Kit; Qiagen). Quantification of the total RNA extracted by NanoDrop (Thermo Fischer Scientific, Waltham, USA). RNA was retrotranscribed using the iScript™cDNA synthesis kit (Bio-Rad Laboratories AG, Cressier FR, Switzerland) according to manufacturer's instructions.

Quantitative real-time PCR

The quantitative real-time PCR was performed using the CFX Connect Real-Time System and the software CFX Manager Version 3.1. Expression level analysis of *Actin* (housekeeping gene), and all candidate genes were performed using the SYBR® Green PCR Master Mix (Applied Biosystems, Carlsbad CA, USA) in combination with corresponding oligonucleotide primers (Supplementary Table 1 and 2).

All amplifications were done in technical duplicates of 5 biological replicates. Using the following thermocycling conditions: 95°C for 10min; 40 cycles of 95°C for 15sec; 60°C for 60sec. Melting curve analysis was performed at 95°C for 15sec, 60°C for 5sec and 95°C for 30sec. Expression levels were calculated using the ΔΔCt method ($2^{-\Delta\Delta Ct}$ formula), after being normalized to the Ct-value of the *Actin* housekeeping gene.

Bioinformatic analysis

Library for bulk seqRNA was prepared using Illumina NovaSeq 6000. Differentially expressed genes were obtained from the DEseq2 output (p.adj <= 0.05) (Supplementary Method 1). We determine pathway enrichment using the ReactomePA v1.38.0 package [39]. We produce a similarity matrix using the Jaccard distance between the enriched terms needed to produce the enrichment map using the R package enrichplot v1.14.1. Raw data available on NCBI/SRA/BioProject database (http://www.ncbi.nlm.nih.gov/bioproject/1067290).

Patients' samples

Samples from patients diagnosed with HPV-negative HNSCC were used under the license BASEC 2018-01729. Tissues from patients 18-90 years old with primary tumor occurrence were collected upon primary surgical therapy performed at the University Hospital Zurich (USZ). Tissues were processed, embedded in OCT and sectioned according to USZ SOPs. For immunohistochemistry staining, primary antibody α-Jagged1 (1:100; Abcam, ab7771) and α-Dll4 (1:100; R&D Systems, AF1389) were used.

Cell culture

The SCC-25 epithelial cell line, derived from the tongue of a 70 years-old OSCC patient, was purchased from the ATCC/LGC company (SCC-25CRL-1628™) and maintained accordingly to

producer indications. Briefly, cells were cultured in DMEM/F12 medium containing 1.2 g/L sodium bicarbonate, 2.5 mM L-glutamine, 15 mM HEPES, 0.5 mM sodium pyruvate (# 11330032, Gibco-ThermoFisher) and 10% fetal bovine serum (#16000044, Gibco-ThermoFisher). Cells were sub-cultured when 80% confluent using trypsin/EDTA (#15400054, Gibco-ThermoFisher) and frozen at 10^6 cells/vial in 10% DMSO (#D4540, Sigma-Aldrich).

Scratch assay

For scratch assay, SCC25 cells were grown to confluence. A central scratch of 1mm of distance was produced using a silicon scraper. Medium was changed immediately with conditioned medium: Control group medium contained the anti-mitotic Aphidicolin (1ug/ml; # A4487 Sigma-Aldrich) and DMSO (#D8418; Sigma-Aldrich); Treated group contained Aphidicolin (1ug/ml; # A4487 Sigma-Aldrich) and CB103 (100µM; # HY-135145 MedChemExpress). Fresh conditioned medium was used for medium changes every two days for 10 days. Images were taken at 20X every day at the same time of the day using a Leica DMIL LED inverted microscope mounting a Leica camera DFC295. Four wells per conditions were analyzed. Quantification of cell-free areas was performed using FIJI/ImageJ free software.

Cell immunofluorescence

Treated SCC25 cells were plated on hatched coverslips at 20.000cells/well. Cells were fixed with PFA4% for 15min at 4°C. After PBS washing, cells were permeabilized 30 min in 0.1% triton and then blocked using a solution of 10% FBS, 0,1% triton in PBS. Primary antibodies were diluted in blocking buffer and incubated overnight. Primary antibodies a-Vinculin 1:500 (#90227 Millipore) was used for immunofluorescence on cells and detected via secondary antibody donkey anti-mouse IgG 546, Alexa Fluor 546 (dilution 1:1000; Invitrogen). Nuclear

counterstaining was performed using DAPI (4',6-Diamidino-2-Phenylindole, Dihydrochloride, #D1306, Invitrogen).

TRITC-conjugated Phalloidin staining of actin filaments was performed as indicated by the manufacturer (1:1000 for 1h incubation at room temperature; Millipore # 90228). Mounting in Mowiol 4-88/Glycerol (#81381 and #G-6279, Sigma-Aldrich).

Time-lapse imaging

Low passage SCC25 cells were treated with CB103 (100µM; # HY-135145 MedChemExpress) or DMSO (#D8418; Sigma-Aldrich) for 4 days and then plated at 10000 cells/well in an 8-wells µ-Slide high glass bottom (#80807, Ibidi). Cells were observed under an Olympus ScanR HCS at 20X with controlled environmental conditions (CO2 5% and 37°C) for 3h, taking an image every 3 minutes. For analysis, Imaris 9.9 (Bitplane) spot and tracking function was used to automatically quantify the displacement length.

Results

Distribution pattern and localization of Notch1, Dll4, and Jag1 in the tongue epithelium

We initially characterized the keratinized stratified epithelium of the tongue for the expression of Notch signaling pathway components. Using the *Notch1*^{CreERT}*:R26mTmG*$^{fl/fl}$ transgenic line, we induced *Notch1*-driven *mGFP* expression upon tamoxifen administration: *mGFP*-expressing cells were identified in the epithelium of the tongue, while unrecombined tissue maintained the expression of the *mTomato* cassette (Figure 1A). Via light-sheet microscopy (mesoSPIM), we generated a three-dimensional reconstruction of the entire tongue epithelium, confirming that *Notch1*-driven *mGFP* is expressed in both the ventral and dorsal parts of the tongue epithelia (Figure 1B, Movie 1). Cross-sections of healthy adult tongues provided a detailed overview of the Notch1 localization in the multilayered epithelium and confirmed its ventral and dorsal expression (Figure 1C). Both the endogenous Notch1 protein and the *Notch1*-driven *mGFP* were expressed from the basal layer up to the stratum granulosum (Figures 1C, 1D). Next, we assessed the distribution of the Jag1 and Dll4 ligands in the tongue epithelium. We found that these two proteins have specific combinatorial expression patterns (Figure 1E and 1F): The Jag1 protein was identified in both the dorsal and ventral sides of the tongue. In the dorsal region, Jag1 staining was observed in the space between the filiform papillae (Figure 1E). In contrast, the Dll4 ligand was exclusively localized in the dorsal part of the tongue epithelium, specifically on the dorsal portion of the filiform papillae (Figure 1F).

Mutually exclusive distribution patterns of Dll4 and Jag1 in the tongue epithelium of OSCC

To model the progressive stages of tongue squamous cell carcinoma, we administered the carcinogenic substance 4-Nitroquinoline N-oxide (4NQO) in the drinking water of 6-weeks-old mice for a duration of 16 weeks (Supplementary Figure 1A). We then analyzed 22 weeks-old and 32 weeks-old mice and performed macroscopic and histological analysis. 22 weeks-old mice showed epithelial hyperplasia, leukoplakia and hyperkeratinization, located predominantly on the dorsal side of the tongue, and rarely in its ventral part (Supplementary Figures 1A, 1B, 1C). 32 weeks-old mice consistently reproduced a papilloma outgrowth on the dorsal epithelium of the tongue (Supplementary Figures 1B, 1C). By contrast, mice receiving DMSO (control group) did not develop any local or systemic pathological condition at any time point analyzed (Supplementary Figures 1B, 1C).

To study the role of Notch in OSCC initiation, we firstly treated *Notch1*^{CreERT}*:R26mTmG*$^{fl/fl}$ mice with 4NQO or DMSO and analyzed the tissue at 22 weeks of age (Figures 2A). Our findings revealed specific expression of *Notch*-driven *mGFP* in the hyperplastic tongue epithelium of 4NQO-treated mice (Figure 2B). Next, we analyzed the distribution of Dll4 and Jag1 molecules at this early time point: Intense Dll4 staining was detected in the hyperplastic tongue epithelium (Figure 2C), whereas Jag1 immunolabelling was absent from that area (Figure 2D; white arrows, and white dashed area). A gradual reduction in Jag1 staining was observed, extending from the neighboring regions bordering the overgrowth (Figure 2D, yellow arrows) to the central core of the tumor mass, where the staining was entirely absent (Figure 2D, white arrows). In contrast, Jag1 staining maintained a physiological pattern of expression in the unaltered regions of the tongue, distant from the hyperplastic area (Figure 2D, red arrows). Staining against the undifferentiation marker SRY-Box Transcription Factor 2 (Sox2) was detected in most cells composing the hyperplastic tongue epithelium (Figure 2E).

We then sought to understand whether the activity of the Notch1-Dll4 signaling axis is a common element during all stages of OSCC progression or is rather confined to the tumor initiation stage. 4NQO-treated *Notch1*^{CreERT}*:R26mTmG*$^{fl/fl}$ transgenic mice were analyzed at later time point (32 weeks-old mice; Figure 3A). The dorsal side of the tongue exhibited a papilloma outgrowth that was labeled with the *Notch*-driven expression of m*GFP* (Figure 3B). At this advanced tumorigenic stage, intense staining for Dll4, but not for Jag1, was detected in the papilloma-forming epithelium (Figures 3C and 3D). Residual Jag1 staining was found in the surrounding areas of the papilloma growth (Figure 3C). To assess the degree of undifferentiation in the tongue papilloma, we conducted staining against the Sox2 and Keratin5 (K5) proteins and identified their presence in the majority of papilloma cells in the 4NQO-treated mice (Supplementary Figures 2A and 2B). By contrast, in DMSO-treated mice, Sox2 and K5 staining was exclusively localized in the basal epithelial layer of the tongue, where undifferentiated progenitors reside (Supplementary Figures 2A and 2B) [40,41]. Staining against Keratin10 (K10), a mature keratinocyte marker [42], was absent from the 4NQO-induced papilloma in the 32-week-old mice (Supplementary Figure 2C). In the DMSO-treated mice, a K10 staining was observed in the tongue's epithelium and was confined to its cornified layer (Supplementary Figure 2C). Staining against the pan-epithelial marker E-Cadherin (E-Cad)[43] labels the surface of the dorsal tongue of DMSO-treated mice. In 4NQO-treated mice, this staining reveals a widespread expression within the tumor overgrowth observed in 32-week-old mice (Supplementary Figure 2D).

Invasive squamous cells conserve their dependency from the Notch1-Dll4 signaling axis

At more advanced stages of OSCC progression, cells of the papilloma outgrowth may become invasive by undergoing epithelial-to-mesenchymal transition (EMT) [44]. To test this hypothesis, we analyzed 38-weeks-old mice expressing *R26:mTomato* treated with 4NQO (Figure 4A).

Sections of the tongues of these animals were stained with the epithelial markers K14 and P63, and the labeling revealed the presence of epithelial cell bulks within tongues' musculature (Figures 4B and 4C). We hypothesized that the papilloma-derived epithelial cells breached the basal lamina and invade the underling connective tissues. To determine whether EMT occurs at this late time point, we analyzed the distribution of the zing-finger transcription factor Snai1 (Snail), known marker for EMT and regulator of the adhesion molecule E-cadherin [45,46]. Snail^{+} staining was observed in cells of the invasive tumor mass in 4NQO-treated mice (Figure 4D, white arrows), while the labeling was absent in DMSO-treated mice (Figure 4D). We further analyzed the distribution of both vimentin and E-cadherin molecules, which are mesenchymal and epithelial markers respectively[46,47]. A subset of cells within the tumor mass were co-stained with vimentin and E-cadherin (Figure 4E, yellow arrows), thus indicating an ongoing EMT process. We therefore sought to clarify if the Notch1-Dll4 signaling axis is also involved in the process of tumor invasion observed in 38-weeks-old mice. *Notch1*^{CreERT}*:R26mTmG*$^{fl/fl}$ mice were used to trace Notch1-expressing cells and their progeny (Figure 5A). In DMSO-treated mice, *mGFP* expression remained restricted to the epithelial layers (Figure 5B). Conversely, in 4NQO-treated mice, mGFP-labeled cells were observed within the carcinoma mass invading the mesenchyme (Figure 5C). We then conducted immunolabelling for the Notch1 protein confirming its presence in the healthy tongue epithelium of 38-weeks-old DMSO-treated mice (Figure 5D). In 4NQO-treated mice, Notch1 staining was identified in both the infiltrating mass and in the distant epithelium (Figure 5D). Finally, we examined the expression of Dll4 in the invasive aberrant epithelium using *R26:mTomato* mice. Analysis of DMSO-treated mice confirmed the expression of Dll4 in the dorsal portion of the filiform papillae, as previously

observed (Figure 5E and 1F). In 4NQO-treated mice, labeling for Dll4 was broadly present in the infiltrating mass (Figure 5E).

Notch-dependent transcription correlates with sustained keratinocytes undifferentiation.

Upon isolation of tongue's epithelium from its underling mesenchyme[38], the total RNA of the epithelium was extracted for sequencing analyses in both 4NQO- and DMSO-treated mice (Figure 6A). We identified 3331 differentially expressed genes in 4NQO-treated versus DMSO-treated epithelia (p-value threshold $p \leq 0.0$; Figure 6 and Supplementary Method 1). Gene Ontology (GO) analysis and Gene Set Enrichment Analysis (GSEA) showed changes in keratinocyte differentiation and cornification processes, in parallel with the regulation of pathways involved in cell fate acquisition and epithelial regeneration (Figure 6B, 6C, 6E and Supplementary Figure 3). Our GSEA analyses in 32-weeks-old mice, detected specific enrichment for the Notch signature (hallmarks and oncogenic signature gene-set databases), in parallel with hallmarks of epithelial-to-mesenchymal transition (EMT) and changes in anchoring junctions (Figure 6F and 6H).

The heatmap shows changes in 2000 genes (Figure 6D) mainly involved in cell differentiation processes (Cluster 2 and Cluster 5), molecular pathways regulating cell fate determination (Cluster 1 and Cluster 5), extracellular matrix rearrangement (Clusters 1,2,3,4), and cell motility (Cluster 3). To confirm the bulk seqRNA analyses, we performed quantitative RT-PCR using mRNA obtained from 4NQO- and DMSO-treated epithelia. 4NQO-treated epithelium showed an important increase in *Dll4* expression compared to DMSO-treated epithelium (Figure 6G). Interestingly, the *Hes*-family of target genes remained largely unaffected, whereas *Hey1* and *Hey2* (Hairy and enhancer of split-related with YPRW motif protein) were significantly reduced in 4NQO-treated epithelia (Figure 6G).

Thereafter, interactome analyses were conducted to examine changes in the tongue's epithelia upon 4NQO and DMSO treatments. Independent *Enrichr (https://maayanlab.cloud/Enrichr/)* analyses identified alteration of *Runt-related transcription factor 1 (Runx1)* amongst others (e.g., *p21, p300* and *Stat3*) (Supplementary Figure 4). Importantly, this alteration is specific to *Runx1*, as other members of the *Runx* family were not significantly altered (Supplementary Figure 4B). As *Runx1* has been previously linked to Notch pathway activation[48–50], we wanted to demonstrate the distribution of the Runx1 protein in the tumorigenic epithelium of the tongue. Indeed, a strong Runx1 staining was detected in the tumor mass of the 4NQO-treated mice (Supplementary Figure 5A), while the Runx1 labelling was confined to the stratum basale and stratum spinosum of the DMSO-treated mice. Furthermore, strong immunostaining against p63, a marker of undifferentiated keratinocytes[51], was detected in the tumor mass of 4NQO-treated mice (Supplementary Figure 5B). In contrast, in DMSO-treated mice, p63 specifically labels the healthy epithelium.[48,52–57]

The Notch signaling pathway regulates malignancy in human OSCC

To assess the clinical relevance of the Notch pathway in human OSCC, we characterized the expression of JAG1 and DLL4 in patients-derived samples. Tissue from HPV-negative adult patients with primary tumor occurrence was first analyzed by H&E staining to identify typical squamous cell carcinoma pathological features (Figure 7A, overview). Dysplastic epithelium, mitotic figures and aberrant keratin accumulation were identified in all samples analyzed (Figure 7A, black arrows). Subsequently, we conducted staining for JAG1 and DLL4 to determine their localization in human samples. We observed a significant variability in the expression of JAG1 among patients, whereas DLL4 consistently appeared in the analyzed aberrant epithelia (Figure 7A). To further characterize the molecular control of the Notch pathway in the human context,

we treated SCC25 cell line (#CRL-1628, ATCC/LGC) with CB103, a pan-blocker of the Notch-transcriptional activation complex[58]. Interestingly, quantitative RT-PCR revealed a specific downregulation of the *DLL4* expression, while *JAG1* levels remain largely unaltered (Figure 7B). Additionally, treatment with CB103 led to a decrease in the expression of *SOX2* and *P63*. (Figure 7B).

To further investigate the functional impact of CB103 treatment, we conducted a scratch assay and monitored the progression of migrating cells over a period of 10 days (Figures 7C and 7D). DMSO-treated cells were able to fully reform the monolayer within a ten-day timeframe, in contrast to CB103-treated cells, which were unable to recolonize the cell-free zone (Figure 7C). As lack of migration could be explained by an increased expression of focal adhesion (FA)[59], we performed vinculin-phalloidin staining and quantify the number of adhesive complexes anchoring epithelial cells to the extracellular matrix[60]. CB103-treated cells displayed a higher number of FA compared to DMSO-treated cells (Figure 7E and 7F). To further confirm the reduced motility of CB103-treated cells, we performed time-lapse analysis. CB103-treated cells exhibited significantly reduced motility when compared to cells treated with DMSO (Figures 7G and 7H; Movies 2 and 3).

Discussion

The Notch signaling pathway is a central regulator of carcinogenic transformation in a variety of epithelial tumors, including lung, cervical, colon, and pancreatic cancers [61–64]. The dysregulation of Notch is context-dependent and can shift from an activator to an inhibitor, depending on the organ and the type of tissue affected [65–67]. Currently, a debate exists on whether the Notch pathway acts as an oncogene or tumor suppressor in OSCC, and its exact role in this type of

cancer remains largely unknown [16,68,69]. In this study, we demonstrate that Notch signaling contributes to OSCC development and progression by preferentially interacting with the Dll4 ligand, while the Jag1 ligand is lost in the malignant outgrowth. This ligand switch occurs in the early stages of hyperplasia and continues to characterize the aberrant tissue in the most advanced stages, including papilloma outgrowth and invasive carcinoma. The selective expression of Jag1/Dll4 can therefore be instrumental in developing new diagnostic tools for the early detection of tongue carcinoma.

The mutually exclusive expression of the Jag1 and Dll4 ligands regulates fate definition and undifferentiation in a variety of tissues (e.g., during angiogenesis and hematopoiesis)[37,70,71]. Similarly, in our study, the selection between the Notch1-Dll4 versus Notch1-Jag1 interaction coincides with sustained keratinocyte undifferentiation. We reasoned that in OSCC, a subset of Notch1/Dll4-expressing keratinocyte progenitors remain in their immature state without advancing into further differentiation steps (i.e., cornification and keratin deposition). This results in the expansion of the undifferentiated portion of the tongue epithelium, which produces a malignant mass that extends outwards and has the capacity to invade the underling connective tissues (e.g., tongue muscles). Therapeutic targeting of Dll4 could therefore have ample relevance to contrast OSCC growth. While Dll4 blockers have been proposed for the treatment of other epithelial tumors (e.g., intestinal tumors)[72] primarily aiming at limiting angiogenesis, it's important to note that OSCC growth is not strictly dependent on vascularization. Therefore, a locally administered blocker could directly target malignant epithelial cells in OSCC. Immunotherapy specifically targeting Dll4 combined to chemotherapy has been applied to treat solid tumors (e.g., pancreatic and lung cancers) [73–76], with positive results spanning from a reduction of tumor growth to a decrease in the reoccurrence rate [77–79].

From a molecular point of view, our study reveals for the first time the downstream changes that occur during Notch pathway dysregulation in OSCC. The preferential binding of Notch1 to Dll4 in the tumorigenic epithelium of the tongue leads to the downregulation of *Hey1* and *Hey2*, while the expression of other Notch-specific target genes such as *Hes1* and *Hes2* remains largely unaffected. Transcriptome analysis revealed a complex scenario of crosstalk between the various signaling pathways sustaining OSCC. Interestingly, *p63* and *Runx1* cooperate with the Notch1-Dll4 signaling axis in OSCC, similarly to what has been found in cells of other tissues (e.g., skin keratinocytes, hematopoietic stem cells) [45,48,49,80–82]. The relevance of these two molecular players in HNSCC has been previously reported. Upregulation of *P63* expression has been correlated with a poor prognosis in OSCC patients [83]. Likewise, *RUNX1* upregulation drives tumor's progression and metastasis, while its suppression inhibits the proliferation and migration of HNSCC cells [84,85,86]. A comparable scenario is observed in our study, where both immunostaining and transcriptomics reveal altered expression of Runx1, Notch1, and Dll4 in OSCC.

Similarly to the findings obtained in mice, Dll4 is regularly expressed in the aberrant epithelium of human-derived cancer samples. To test the functional effect of Notch pharmacological inhibition in the context of human OSCC, we treated the SCC25 cell line with the Notch blocker CB103 [58]. CB103 is increasingly gathering attention in cancer treatments, in view of its high stability and unbeaten specificity in targeting the Notch pathway [87,88]. Several clinical trials are currently in place to determine its usage as a therapeutic agent in carcinomas (clinical trials: NCT03422679, NCT04714619) as well as leukemias and lymphomas (clinical trials: NCT03422679, NCT05464836). In our system, SCC25 cells treated with CB103 displayed a significant reduction in *DLL4* expression, with no observable change in *JAG1* expression,

confirming the crucial role of the Notch-Dll4 signaling axis in OSCC. Importantly, the expression of the undifferentiation markers *SOX2* and *P63* is notably reduced in CB103-treated cells, thus indicating that the undifferentiated state of cancer cells is Notch signaling-dependent. These *in vitro* results validate the *in vivo* findings in mice and denote the connection between an active Notch-Dll4 signaling axis and the prolonged undifferentiation cell state within OSCC. Moreover, the dramatic effect of CB103 on SCC25 cells migration, accompanied by an increased number of focal adhesions, suggests that Notch is important for the acquisition of the invasive phenotype of the tumor.

In conclusion, the present findings show that the Notch1-Dll4 signaling axis plays a crucial role in the initiation and development of OSCC and indicate that this oncogenic action could be successfully blocked upon targeted pharmacologic treatment.

Author contribution statement

C.P. and T.A.M conceptualized and designed the project. C.T.M, R.D., N.R., I.J.V., C.P. carried out the experiments. C.T.M, N.R., A.B., T.A.M. and C.P. analyzed data. T.A.M. and C.P provided financial and administrative support. C.P. and T.A.M. supervised the project. C.P., C.T.M and T.A.M. wrote the manuscript.

Acknowledgements

This work was supported by the University of Zurich, the Krebsliga (KFS-4890-08-2019-R) (T.A.M.) and the Olga Mayenfisch Stiftung (C.P.). We thank Prof. Spyros Artavanis-Tsakonas (Harvard Medical School, Harvard University) for providing *Notch1*^{creER} mice.

Imaging was performed with equipment maintained by the Center for Microscopy and Image Analysis, University of Zurich. The authors gratefully acknowledge the Functional Genomics Center Zurich (FGCZ) of University of Zurich and ETH Zurich for the support on analyses.

References

1. Ferlay, J. *et al.* Estimating the global cancer incidence and mortality in 2018: GLOBOCAN sources and methods. *Int J Cancer* **144**, 1941–1953 (2019).
2. Bray, F. *et al.* Global cancer statistics 2018: GLOBOCAN estimates of incidence and mortality worldwide for 36 cancers in 185 countries. *CA: A Cancer Journal for Clinicians* **68**, 394–424 (2018).
3. Johnson, D. E. *et al.* Head and neck squamous cell carcinoma. *Nat Rev Dis Primers* **6**, 92 (2020).
4. Cramer, J. D., Burtness, B., Le, Q. T. & Ferris, R. L. The changing therapeutic landscape of head and neck cancer. *Nat Rev Clin Oncol* **16**, 669–683 (2019).
5. Duprez, F. *et al.* Distant metastases in head and neck cancer: Distant metastases in head and neck cancer. *Head & Neck* **39**, 1733–1743 (2017).
6. Pisani, P. *et al.* Metastatic disease in head & neck oncology. *Acta Otorhinolaryngol Ital* **40**, S1–S86 (2020).
7. Müller, S. Update from the 4th Edition of the World Health Organization of Head and Neck Tumours: Tumours of the Oral Cavity and Mobile Tongue. *Head Neck Pathol* **11**, 33–40 (2017).
8. Pai, S. I. & Westra, W. H. Molecular pathology of head and neck cancer: implications for diagnosis, prognosis, and treatment. *Annu Rev Pathol* **4**, 49–70 (2009).
9. Byers, R. M. *et al.* Frequency and therapeutic implications of ‘skip metastases’ in the neck from squamous carcinoma of the oral tongue. *Head Neck* **19**, 14–19 (1997).
10. Kuperman, D. I. *et al.* Squamous cell cancer of the head and neck with distant metastasis at presentation. *Head Neck* **33**, 714–718 (2011).

11. Califano, J. *et al.* Genetic progression and clonal relationship of recurrent premalignant head and neck lesions. *Clin Cancer Res* **6**, 347–352 (2000).
12. Puram, S. V. *et al.* Cellular states are coupled to genomic and viral heterogeneity in HPV-related oropharyngeal carcinoma. *Nat Genet* **55**, 640–650 (2023).
13. Bai, Y. *et al.* YBX1 integration of oncogenic PI3K/mTOR signalling regulates the fitness of malignant epithelial cells. *Nat Commun* **14**, 1591 (2023).
14. Stransky, N. *et al.* The Mutational Landscape of Head and Neck Squamous Cell Carcinoma. *Science* **333**, 1157–1160 (2011).
15. Sequeira, I. *et al.* Genomic landscape and clonal architecture of mouse oral squamous cell carcinomas dictate tumour ecology. *Nat Commun* **11**, 5671 (2020).
16. Agrawal, N. *et al.* Exome sequencing of head and neck squamous cell carcinoma reveals inactivating mutations in NOTCH1. *Science* **333**, 1154–1157 (2011).
17. Fan, W.-L. *et al.* Prognostic Genetic Biomarkers Based on Oncogenic Signaling Pathways for Outcome Prediction in Patients with Oral Cavity Squamous Cell Carcinoma. *Cancers (Basel)* **13**, 2709 (2021).
18. Loganathan, S. K. *et al.* Rare driver mutations in head and neck squamous cell carcinomas converge on NOTCH signaling. *Science* **367**, 1264–1269 (2020).
19. Artavanis-Tsakonas, S. Notch Signaling: Cell Fate Control and Signal Integration in Development. *Science* **284**, 770–776 (1999).
20. Casey, L. M. *et al.* Jag2-Notch1 signaling regulates oral epithelial differentiation and palate development. *Dev. Dyn.* **235**, 1830–1844 (2006).
21. Mustonen, T. *et al.* Lunatic fringe, FGF, and BMP regulate the Notch pathway during epithelial morphogenesis of teeth. *Dev Biol* **248**, 281–293 (2002).

22. Mitsiadis, T. A., Henrique, D., Thesleff, I. & Lendahl, U. Mouse Serrate-1 (Jagged-1): expression in the developing tooth is regulated by epithelial-mesenchymal interactions and fibroblast growth factor-4. *Development* **124**, 1473–1483 (1997).

23. Mitsiadis, T. A., Lardelli, M., Lendahl, U. & Thesleff, I. Expression of Notch 1, 2 and 3 is regulated by epithelial-mesenchymal interactions and retinoic acid in the developing mouse tooth and associated with determination of ameloblast cell fate. *Journal of Cell Biology* **130**, 407–418 (1995).

24. Porcheri, C. & Mitsiadis, T. A. Notch in Head and Neck Cancer. *Adv Exp Med Biol* **1287**, 81–103 (2021).

25. Artavanis-Tsakonas, S., Rand, M. D. & Lake, R. J. Notch signaling: cell fate control and signal integration in development. *Science* **284**, 770–776 (1999).

26. Kopan, R. & Ilagan, M. X. G. The canonical Notch signaling pathway: unfolding the activation mechanism. *Cell* **137**, 216–233 (2009).

27. Gordon, W. R., Arnett, K. L. & Blacklow, S. C. The molecular logic of Notch signaling--a structural and biochemical perspective. *J Cell Sci* **121**, 3109–3119 (2008).

28. Siebel, C. & Lendahl, U. Notch Signaling in Development, Tissue Homeostasis, and Disease. *Physiological Reviews* **97**, 1235–1294 (2017).

29. Louvi, A. & Artavanis-Tsakonas, S. Notch and disease: A growing field. *Seminars in Cell & Developmental Biology* **23**, 473–480 (2012).

30. Yoshida, R. *et al*. The pathological significance of Notch1 in oral squamous cell carcinoma. *Lab. Invest.* **93**, 1068–1081 (2013).

31. Setoguchi. Upregulation of Notch pathway molecules in oral squamous cell carcinoma. *Int J Oncol* **36**, (2010).

32. Sakamoto, K. *et al*. Reduction of NOTCH1 expression pertains to maturation abnormalities of keratinocytes in squamous neoplasms. *Laboratory Investigation* **92**, 688–702 (2012).
33. Sawangarun, W. *et al.* Loss of Notch1 predisposes oro-esophageal epithelium to tumorigenesis. *Experimental Cell Research* **372**, 129–140 (2018).
34. Natsuizaka, M. *et al.* Interplay between Notch1 and Notch3 promotes EMT and tumor initiation in squamous cell carcinoma. *Nat Commun* **8**, 1758 (2017).
35. Fre, S. *et al*. Notch lineages and activity in intestinal stem cells determined by a new set of knock-in mice. *PLoS One* **6**, e25785 (2011).
36. Muzumdar, M. D., Tasic, B., Miyamichi, K., Li, L. & Luo, L. A global double-fluorescent Cre reporter mouse. *Genesis* **45**, 593–605 (2007).
37. Porcheri, C. *et al.* Notch ligand Dll4 impairs cell recruitment to aortic clusters and limits blood stem cell generation. *EMBO J.* **39**, e104270 (2020).
38. Meisel, C. T., Pagella, P., Porcheri, C. & Mitsiadis, T. A. Three-Dimensional Imaging and Gene Expression Analysis Upon Enzymatic Isolation of the Tongue Epithelium. *Front Physiol* **11**, 825 (2020).
39. Yu, G. & He, Q.-Y. ReactomePA: an R/Bioconductor package for reactome pathway analysis and visualization. *Mol. BioSyst.* **12**, 477–479 (2016).
40. Vasca, V. *et al.* Keratin 5 expression in squamocellular carcinoma of the head and neck. *Oncol Lett* **8**, 2501–2504 (2014).
41. Alam, H., Sehgal, L., Kundu, S. T., Dalal, S. N. & Vaidya, M. M. Novel function of keratins 5 and 14 in proliferation and differentiation of stratified epithelial cells. *Mol Biol Cell* **22**, 4068–4078 (2011).

42. Sanz-Gómez, N. *et al.* Squamous differentiation requires G2/mitosis slippage to avoid apoptosis. *Cell Death Differ* **27**, 2451–2467 (2020).

43. Huntsman, D. G. & Caldas, C. Assignment1 of the E-cadherin gene (CDH1) to chromosome 16q22.1 by radiation hybrid mapping. *Cytogenet Cell Genet* **83**, 82–83 (1998).

44. González, M. M. *et al.* Is cancer a pure growth curve or does it follow a kinetics of dynamical structural transformation? *BMC Cancer* **17**, 174 (2017).

45. Villarejo, A., Cortés-Cabrera, A., Molina-Ortíz, P., Portillo, F. & Cano, A. Differential role of Snail1 and Snail2 zinc fingers in E-cadherin repression and epithelial to mesenchymal transition. *J Biol Chem* **289**, 930–941 (2014).

46. Thiery, J. P. Epithelial–mesenchymal transitions in tumour progression. *Nat Rev Cancer* **2**, 442–454 (2002).

47. Dongre, A. & Weinberg, R. A. New insights into the mechanisms of epithelial–mesenchymal transition and implications for cancer. *Nat Rev Mol Cell Biol* **20**, 69–84 (2019).

48. Burns, C. E., Traver, D., Mayhall, E., Shepard, J. L. & Zon, L. I. Hematopoietic stem cell fate is established by the Notch-Runx pathway. *Genes Dev.* **19**, 2331–2342 (2005).

49. Burns, C. E. & Zon, L. I. Notch Signaling Is Necessary and Sufficient for Runx1-Dependent Stem Cell Induction in the Embryonic Aorta-Gonad-Mesonephros (AGM) Region. *Blood* **104**, 4161–4161 (2004).

50. Islam, R. *et al.* RUNX1 colludes with NOTCH1 to reprogram chromatin in T cell acute lymphoblastic leukemia. *iScience* **26**, 106795 (2023).

51. Crum, C. P. & McKeon, F. D. p63 in epithelial survival, germ cell surveillance, and neoplasia. *Annu Rev Pathol* **5**, 349–371 (2010).

52. Srivastava, S. S. *et al*. Keratin 5/14□mediated cell differentiation and transformation are regulated by TAp63 and Notch□1 in oral squamous cell carcinoma□derived cells. *Oncol Rep* **39**, 2393–2401 (2018).
53. Dotto, G. P. Crosstalk of Notch with p53 and p63 in cancer growth control. *Nat Rev Cancer* **9**, 587–595 (2009).
54. Moses, M. A. *et al*. Molecular Mechanisms of p63-Mediated Squamous Cancer Pathogenesis. *Int J Mol Sci* **20**, E3590 (2019).
55. Ortt, K., Raveh, E., Gat, U. & Sinha, S. A chromatin immunoprecipitation screen in mouse keratinocytes reveals Runx1 as a direct transcriptional target of DeltaNp63. *J Cell Biochem* **104**, 1204–1219 (2008).
56. Nakagawa, M. *et al.* AML1/Runx1 rescues Notch1-null mutation-induced deficiency of para-aortic splanchnopleural hematopoiesis. *Blood* **108**, 3329–3334 (2006).
57. Kouwenhoven, E. N. *et al.* Transcription factor p63 bookmarks and regulates dynamic enhancers during epidermal differentiation. *EMBO Rep* **16**, 863–878 (2015).
58. Lehal, R. *et al.* Pharmacological disruption of the Notch transcription factor complex. *Proc Natl Acad Sci U S A* **117**, 16292–16301 (2020).
59. Ilić, D. *et al.* Reduced cell motility and enhanced focal adhesion contact formation in cells from FAK-deficient mice. *Nature* **377**, 539–544 (1995).
60. Geiger, B., Tokuyasu, K. T., Dutton, A. H. & Singer, S. J. Vinculin, an intracellular protein localized at specialized sites where microfilament bundles terminate at cell membranes. *Proc Natl Acad Sci U S A* **77**, 4127–4131 (1980).
61. Avila, J. L. & Kissil, J. L. Notch signaling in pancreatic cancer: oncogene or tumor suppressor? *Trends Mol Med* **19**, 320–327 (2013).

62. Brzozowa-Zasada, M. *et al.* Notch and its oncogenic activity in human malignancies. *Eur Surg* **49**, 199–209 (2017).

63. Tyagi, A., Sharma, A. K. & Damodaran, C. A Review on Notch Signaling and Colorectal Cancer. *Cells* **9**, E1549 (2020).

64. Rodrigues, C., Joy, L. R., Sachithanandan, S. P. & Krishna, S. Notch signalling in cervical cancer. *Exp Cell Res* **385**, 111682 (2019).

65. Dotto, G. P. Notch tumor suppressor function. *Oncogene* **27**, 5115–5123 (2008).

66. Yap, L. *et al.* The opposing roles of NOTCH signalling in head and neck cancer: a mini review. *Oral Dis* **21**, 850–857 (2015).

67. Fukusumi, T. & Califano, J. A. The NOTCH Pathway in Head and Neck Squamous Cell Carcinoma. *J Dent Res* **97**, 645–653 (2018).

68. Cancer Genome Atlas Network. Comprehensive genomic characterization of head and neck squamous cell carcinomas. *Nature* **517**, 576–582 (2015).

69. Johnson, D. E. *et al.* Head and neck squamous cell carcinoma. *Nat Rev Dis Primers* **6**, 92 (2020).

70. Benedito, R. *et al.* The notch ligands Dll4 and Jagged1 have opposing effects on angiogenesis. *Cell* **137**, 1124–1135 (2009).

71. Gama-Norton, L. *et al.* Notch signal strength controls cell fate in the haemogenic endothelium. *Nat Commun* **6**, 8510 (2015).

72. Ridgway, J. *et al.* Inhibition of Dll4 signalling inhibits tumour growth by deregulating angiogenesis. *Nature* **444**, 1083–1087 (2006).

73. Hidalgo, M. *et al.* A phase 1b study of the anti-cancer stem cell agent demcizumab (DEM) and gemcitabine (GEM) +/- nab-paclitaxel in patients with pancreatic cancer. *JCO* **34**, 341–341 (2016).

74. McKeage, M. J. *et al.* Phase IB Trial of the Anti-Cancer Stem Cell DLL4-Binding Agent Demcizumab with Pemetrexed and Carboplatin as First-Line Treatment of Metastatic Non-Squamous NSCLC. *Target Oncol* **13**, 89–98 (2018).

75. Coleman, M. L. *et al.* Asparaginyl hydroxylation of the Notch ankyrin repeat domain by factor inhibiting hypoxia-inducible factor. *J Biol Chem* **282**, 24027–24038 (2007).

76. Johnson, M. *et al.* Abstract A081: A phase 1b, open-label, dose escalation and expansion study of demcizumab plus pembrolizumab in patients with locally advanced or metastatic solid tumors. in *Clinical Trials* A081–A081 (American Association for Cancer Research, 2018). doi:10.1158/1535-7163.TARG-17-A081.

77. Fischer, M. *et al.* Anti-DLL4 inhibits growth and reduces tumor-initiating cell frequency in colorectal tumors with oncogenic KRAS mutations. *Cancer Res.* **71**, 1520–1525 (2011).

78. Yen, W.-C. *et al.* Anti-DLL4 Has Broad Spectrum Activity in Pancreatic Cancer Dependent on Targeting DLL4-Notch Signaling in Both Tumor and Vasculature Cells. *Clin Cancer Res* **18**, 5374–5386 (2012).

79. Smith, D. C. *et al.* A Phase I Dose Escalation and Expansion Study of the Anticancer Stem Cell Agent Demcizumab (Anti-DLL4) in Patients with Previously Treated Solid Tumors. *Clinical Cancer Research* **20**, 6295–6303 (2014).

80. Nguyen, B.-C. *et al.* Cross-regulation between Notch and p63 in keratinocyte commitment to differentiation. *Genes Dev* **20**, 1028–1042 (2006).

81. Ichikawa, M. *et al.* A role for RUNX1 in hematopoiesis and myeloid leukemia. *Int J Hematol* **97**, 726–734 (2013).

82. Gao, L. *et al.* RUNX1 and the endothelial origin of blood. *Exp Hematol* **68**, 2–9 (2018).

83. Loljung, L. *et al.* High expression of p63 is correlated to poor prognosis in squamous cell carcinoma of the tongue. *J Oral Pathol Med* **43**, 14–19 (2014).

84. Feng, X. *et al.* Elevated RUNX1 is a prognostic biomarker for human head and neck squamous cell carcinoma. *Exp Biol Med (Maywood)* **246**, 538–546 (2021).

85. Liu, K. *et al.* RUNX1 promotes MAPK signaling to increase tumor progression and metastasis via OPN in head and neck cancer. *Carcinogenesis* **42**, 414–422 (2021).

86. Feng, X. *et al.* Elevated RUNX1 is a prognostic biomarker for human head and neck squamous cell carcinoma. *Exp Biol Med (Maywood)* **246**, 538–546 (2021).

87. Fabbro, D., Bauer, M., Murone, M. & Lehal, R. Notch Inhibition in Cancer: Challenges and Opportunities. *Chimia (Aarau)* **74**, 779–783 (2020).

88. Perez Garcia, J. M. *et al.* First-in-human phase 1-2A study of CB-103, an oral Protein-Protein Interaction Inhibitor targeting pan-NOTCH signalling in advanced solid tumors and blood malignancies. *JCO* **36**, TPS2619–TPS2619 (2018).

Figures

Figure 1: Tongue keratinocytes express components of the Notch signaling pathway.

A) Schematic representation illustrating the murine tongue of a *Notch1*^{CreERT}*:R26mTmG*$^{fl/fl}$ mouse after tamoxifen induction and subsequent *mGFP* expression. Unrecombined tissue in the mouse tongue expresses the *mTomato* cassette. B) mesoSPIM imaging and related three-dimensional reconstruction of a whole-mount *Notch1*^{CreERT}*:R26mTmG*$^{fl/fl}$ mouse tongue. Notch1-driven *mGFP* expression (green) in the raw reconstruction (left panels) and relative surface rendering (right panels). C) Cross-sections of the dorsal (left panels) and ventral (right panels) part of the tongue stained against Notch1 full length (green). Nuclear counterstaining with DAPI (blue). (*) indicates magnified area in the corresponding region of the overview. D) Cross-sections displaying the dorsal (left panel) and ventral part (right panel) of the tongue of a *Notch1*^{CreERT}*:R26mTmG*$^{fl/fl}$ mouse. Notch1-driven *mGFP* was found in both the dorsal and ventral epithelium (green). Unrecombined tissue expressed *mTomato* (red). Nuclear counterstaining with DAPI (blue). (*) indicates magnified area in the corresponding region of the overview. E) Cross-sections illustrating the dorsal (left panel) and ventral (right panel) parts of the tongue stained against Jag1 (green), and DAPI (blue). F) Cross-sections illustrating the dorsal (left panel) and ventral (right panel) parts of the tongue stained against Dll4 (green), and DAPI (blue). Scale bars in overviews100µm. Scale bars in magnification 50µm.

Figure 2: Distribution of Jag1 and Dll4 is mutually exclusive in the early stage of OSCC

(A) Schematic representation illustrating the tamoxifen induction and treatment paradigm with 4NQO or DMSO in 22-week-old *Notch1*^{CreERT}*:R26mTmG*$^{fl/fl}$ mice. (B) Cross-sections displaying the dorsal part of the tongue of a *Notch1*^{CreERT}*:R26mTmG*$^{fl/fl}$ mouse treated with DMSO (upper

panels) or 4NQO (lower panels). Notch1-driven *mGFP* was found in the normal and aberrant epithelium (green). Unrecombined tissue expressed *mTomato* (red). Nuclear counterstaining with DAPI (blue). (*) and (**) Indicate magnified areas in the corresponding regions of the overview. (C) Cross-sections of the dorsal part of the tongue stained against Dll4 (green) in DMSO- (upper panels) and 4NQO-treated mice (lower panels). Nuclear counterstaining with DAPI (blue). (D) Cross-sections displaying the dorsal part of the tongue stained against Jag1(green) and DAPI (blue) after 4NQO/DMSO treatment. A gradient of Jag1 expression is noticeable in the 4NQO-treated epithelium: Jag1 is maintained in the epithelium distant from the lesion (red arrows), is reduced in the epithelium closer to the lesion (yellow arrows) and is absent in the hyperplastic mass (white arrows). Dashed line indicates the border of the hyperplastic region. (E) Cross-sections displaying the dorsal part of the tongue stained against SOX2 (green) and DAPI (blue) after 4NQO/DMSO treatment. (*) Indicates magnified area in the corresponding region of the overview. Scale bars in overviews100µm. Scale bars in magnification 50µm.

Figure 3: Dll4 is specifically expressed in OSCC' papilloma mass

(A) Schematic representation illustrating the tamoxifen induction and treatment paradigm with 4NQO or DMSO in 32-week-old *Notch1CreERT:R26mTmGfl/fl* mice. (B) Cross-sections displaying the dorsal part of the tongue of a *Notch1*^{CreERT}*:R26mTmG*$^{fl/fl}$ mouse treated with DMSO (upper panels). Cross-sections displaying the dorsal part of the tongue of a *Notch1*^{CreERT}*:R26mTmG*$^{fl/fl}$ mouse treated with 4NQO (lower panels). Broad expression of *mGFP* is detected in the whole papilloma mass. Unrecombined tissue expressed *mTomato* (red). Nuclear counterstaining with DAPI (blue). (*) (**) (***) Indicate magnified areas in the corresponding regions of the overview. (C) Cross-sections of the dorsal part of the tongue stained against Jag1 (green) in DMSO- (left panels) and 4NQO-treated mice (right panels). Nuclear counterstaining with DAPI (blue). (*) and (**) Indicate magnified areas in the corresponding regions of the overview. Dashed line indicates the border of the papilloma region. (D) Cross-sections of the dorsal part of the tongue stained against Dll4 (green) in DMSO- (left panels) and 4NQO-treated mice (right panels). Nuclear counterstaining with DAPI (blue). (*) and (**) Indicate magnified areas in the corresponding regions of the overview. Dashed line indicates the border of the papilloma region. Scale bars in overviews 100µm. Scale bars in magnification 50µm.

Figure 4: Epithelial cells invade the adjacent mesenchymal tissue

(A) Schematic representation illustrating the treatment paradigm with 4NQO or DMSO in 38-week-old mice. (B) Cross-sections displaying the dorsal part of the tongue labelled with the pan-epithelial marker K14 (cyan) in DMSO-treated (left panels) and 4NQO-treated mice (right panels). Unrecombined tissue expressed *mTomato* (red). (*) and (**) Indicate magnified area in the corresponding regions of the overview. (C) Cross-sections displaying the dorsal part of the

tongue labelled with the keratinocytes marker P63 (cyan) in DMSO-treated (left panels) vs 4NQO-treated (right panels) conditions. Unrecombined tissue expressed *mTomato* (red). (*) and (**) Indicate magnified areas in the corresponding regions of the overview. (D) Cross-sections displaying the dorsal part of the tongue labelled with the suppressor of transcription SNAIL (cyan) in DMSO-treated (left panel) and 4NQO-treated condition (right panels). (*) Indicates magnified area in the corresponding region of the overview. White arrows indicate Snail+ cells. Nuclear counterstaining with DAPI (blue). (E) Cross-sections displaying the dorsal part of the tongue stained for the mesenchymal marker Vimentin and the epithelial marker E-Cadherin in DMSO-treated (left panel) and 4NQO-treated (right panels) conditions. (*) and (**) Indicate magnified areas in the corresponding regions of the overview. White arrows indicate single positivity for Vimentin. Yellow arrows indicate double positivity for Vimentin and E-cadherin. Nuclear counterstaining with DAPI (blue). (*) Indicates magnified area in the corresponding region of the overview. Scale bars in overviews 100µm. Scale bars in magnification 50µm.

Figure 5: Notch1^{+} cells invade neighboring non-epithelial tissue

(A) Schematic representation illustrating the tamoxifen induction and treatment paradigm with 4NQO or DMSO in 38-week-old *Notch1^{CreER}T:R26mTmG$^{fl/fl}$* mice. (B) Cross-sections displaying the Notch1-driven expression of *mGFP* in DMSO-treated epithelium. Unrecombined tissue expressed *mTomato* (red). Nuclear counterstaining with DAPI (blue). (*) Indicates magnified area in the corresponding region of the overview. (C) Tongue cross-sections displaying the Notch1-driven expression of *mGFP* in 4NQO-treated mice ten days post tamoxifen induction. Unrecombined tissue expressed *mTomato* (red). Nuclear counterstaining with DAPI (blue). (*) and (**) Indicate magnified area in the corresponding regions of the overview. (D) Cross-

sections displaying the endogenous Notch1-full length expression (cyan) in DMSO- (left panels) and 4NQO-treated tissues (right panels). Unrecombined tissue expressed *mTomato* (red). (*) and (**) Indicate magnified area in the corresponding regions of the overview. (E) Cross-sections displaying the endogenous Dll4 expression (green) in DMSO- (left panels) and 4NQO-treated tissues (right panels). (*) Indicates magnified area in the corresponding region of the overview. Dashed lines identify the infiltrated area inside the muscular mesenchyme. Scale bars in overviews 100µm. Scale bars in magnification 50µm.

Figure 6: Transcriptome analyses of differentially expressed genes in cancerogenic versus control conditions

(A) Schematic representation of epithelium separation for RNA isolation and follow up analysis[38]. (B,C) Gene Ontology (GO) enrichment analyses showing alterations in keratin differentiation and cornification in both Cellular Components (CC) and Biological Processes (BP) domains. (D) Heatmap depicting changes of gene expression between 4NQO and DMSO conditions with hierarchical clustering. (E) Gene Set Enrichment Analysis (GSEA) confirms alterations in the process of keratinization when comparing 4NQO vs DMSO conditions. (F) Enrichment plot for the Notch-signaling signature via Gene Set Enrichment Analysis (GSEA). (G) Independent qRT-PCR confirms the overexpression of *Dll4* and downregulation of the Notch effectors *Hey1* and *Hey2* in 4NQO condition. Error bars indicate standard error. *=$p<0.05$; **=$p<0.01$; ***=$p<0.001$ (H) Gene Set Enrichment Analysis (GSEA) reveal a signature for epithelial-to-mesenchymal transition and alteration of the anchoring junctions when comparing 4NQO vs DMSO transcriptome.

Figure 7: The Notch signaling pathway regulates malignancy in human squamous cell carcinoma

(A) Histological examination of human squamous cell carcinoma tissue. Hematoxylin/Eosin staining is used to identify aberrant histology in two representative patients (Patient#1 left panel, Patient#2 right panel). Black arrows indicate aberrant features characteristics of squamous cell carcinoma. Expression of Jagged1 and Dll4 is shown in magnified areas (∗: Patient#1; ∗∗: Patient#2). Scale bar in magnification: 100µm. Scale bar in overview: 1mm. (B) qRT-PCR on SCC25 human cell line treated with DMSO (control) or the Notch-blocker (CB103). CB103-treatment significantly affects *Dll4* expression with minimal changes in *Jagged1* expression. Blockage of Notch-specific transcriptional control importantly reduces the expression of the undifferentiated markers *Sox2* and *P63*. C) Scratch assay on SCC25 cells treated with DMSO or CB103. Scale bar 100µm. (D) Quantification of cell-free zone in the scratch assay. Each condition was normalized with the cell-free scratched area on day0. Error bars indicate standard error. **=p<0.01; ***=p<0.001; ****=p<0.0001 E) Representative images for actin filaments and focal adhesions immunofluorescence. Green staining: phalloidin. Red staining: Vinculin. Blue staining: DAPI. Scale bar 10µm. (F) Quantification of the number of focal adhesion complexes in each cell. ***=p<0.001 (G) Time lapse analyses on SCC25 cells treated with DMSO or CB103. Single snapshots for representative footages over 2h25 recording. Related to Movie 2 and Movie 3. Scale bar 50µm. H) Quantification of displacement length for each cell via Imaris software (spot tracking). ***=p<0.001

Graphical Abstract

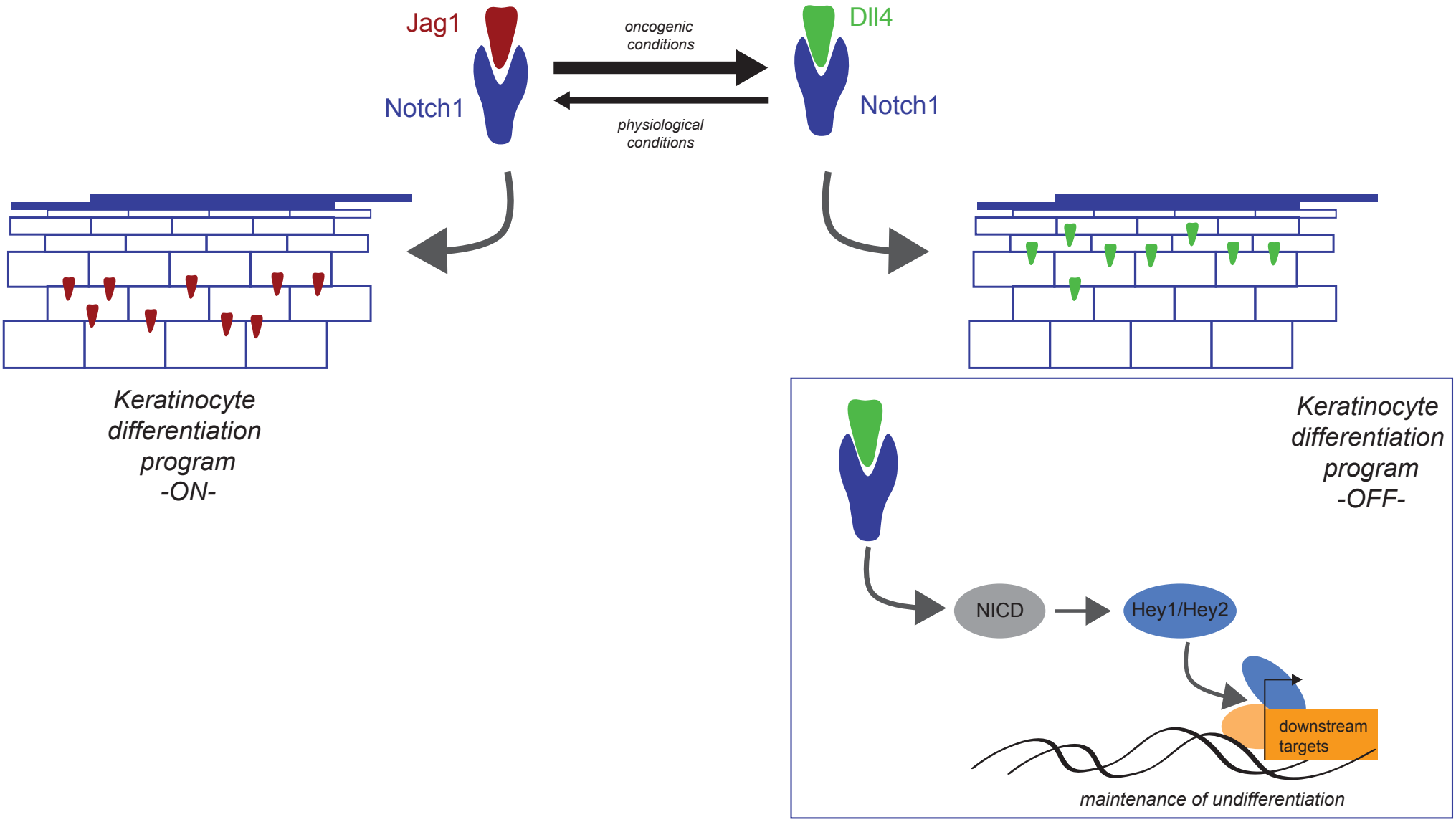

Figure 1: Tongue keratinocytes express components of the Notch signaling pathway.

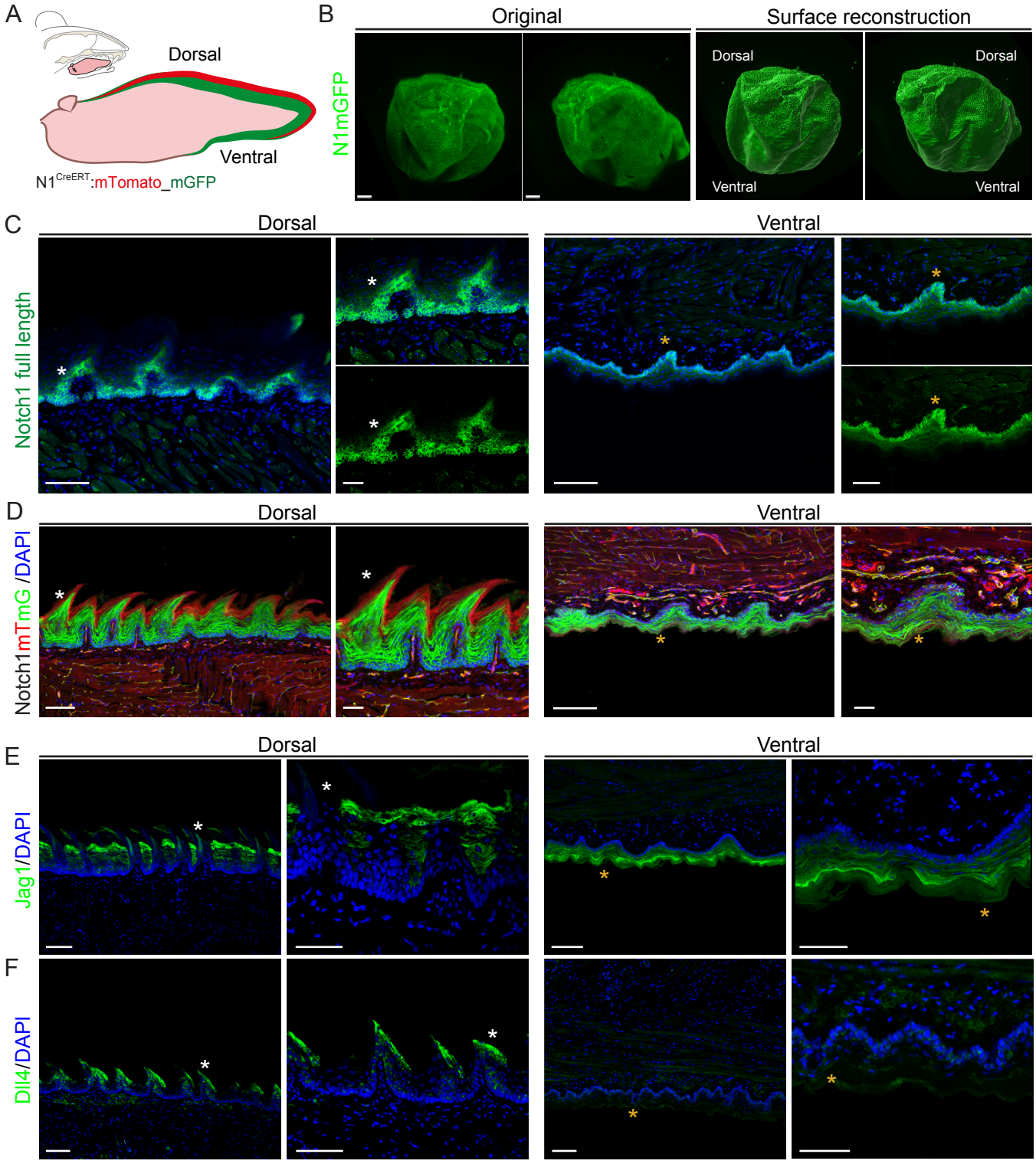

Figure 2: Distribution of Jag1 and Dll4 is mutually exclusive in the early stage of OSCC

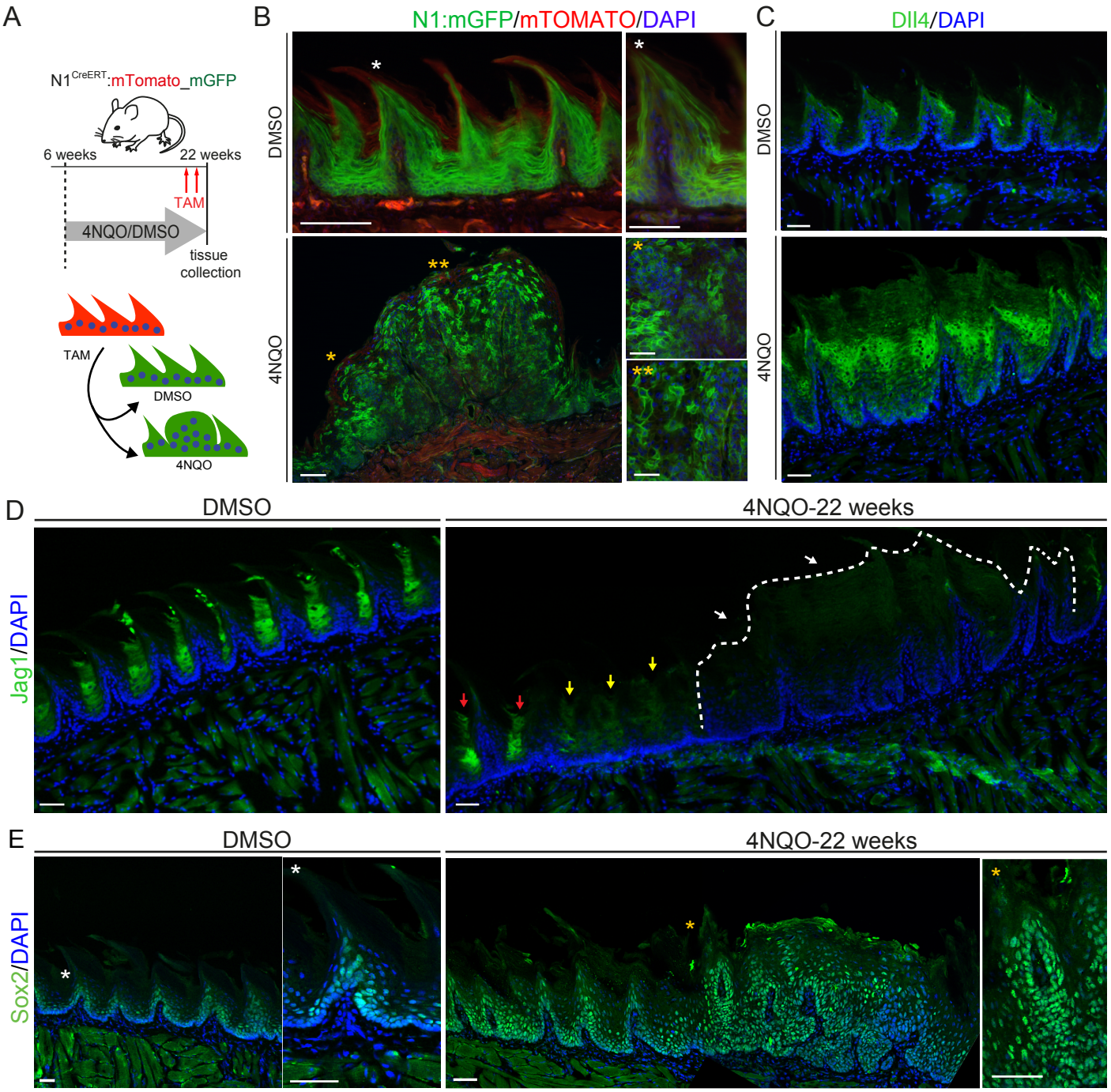

Figure 3: Dll4 is specifically expressed in OSCC' papilloma mass

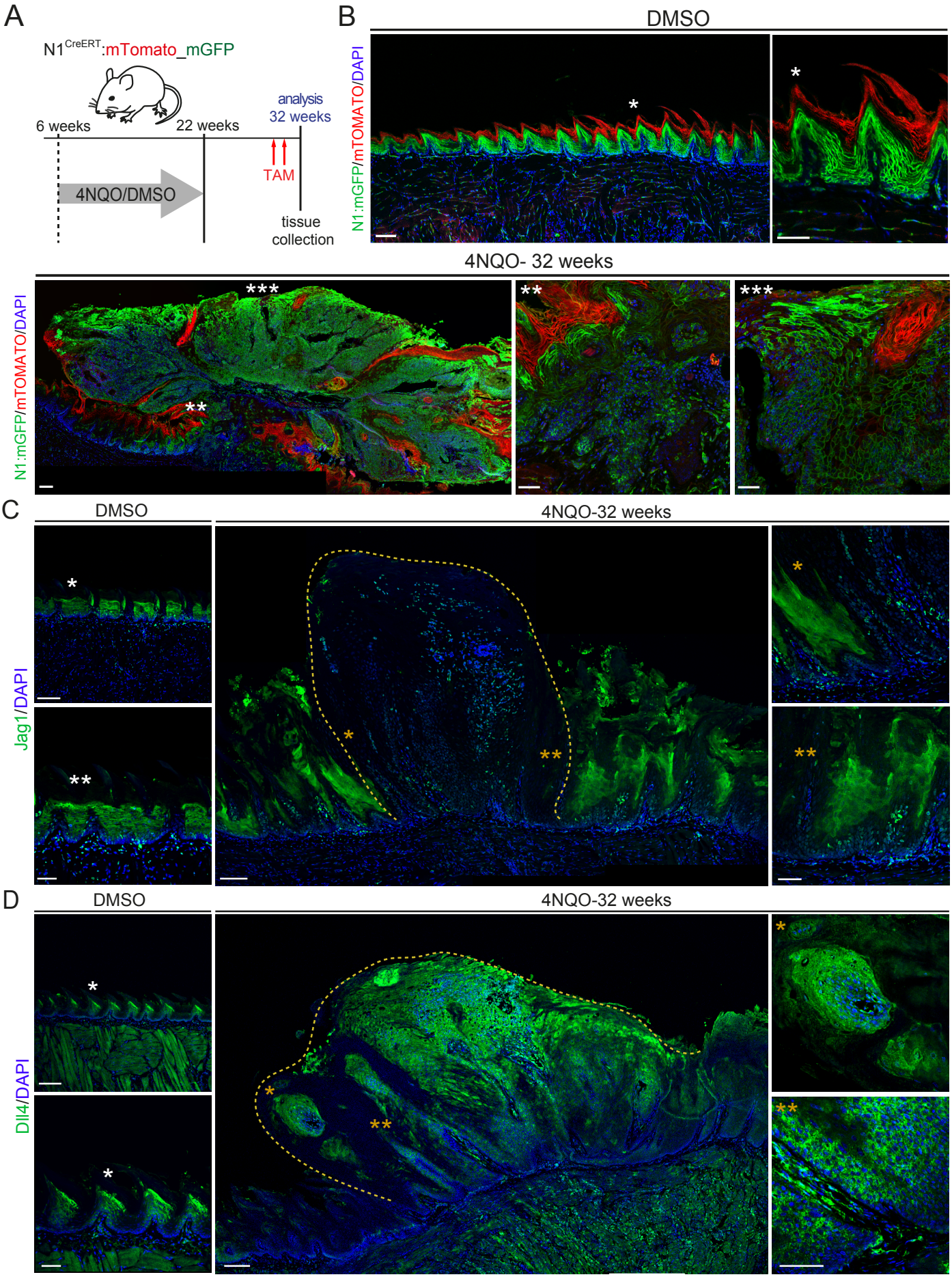

Figure 4: Epithelial cells invade the adjacent mesenchymal tissue

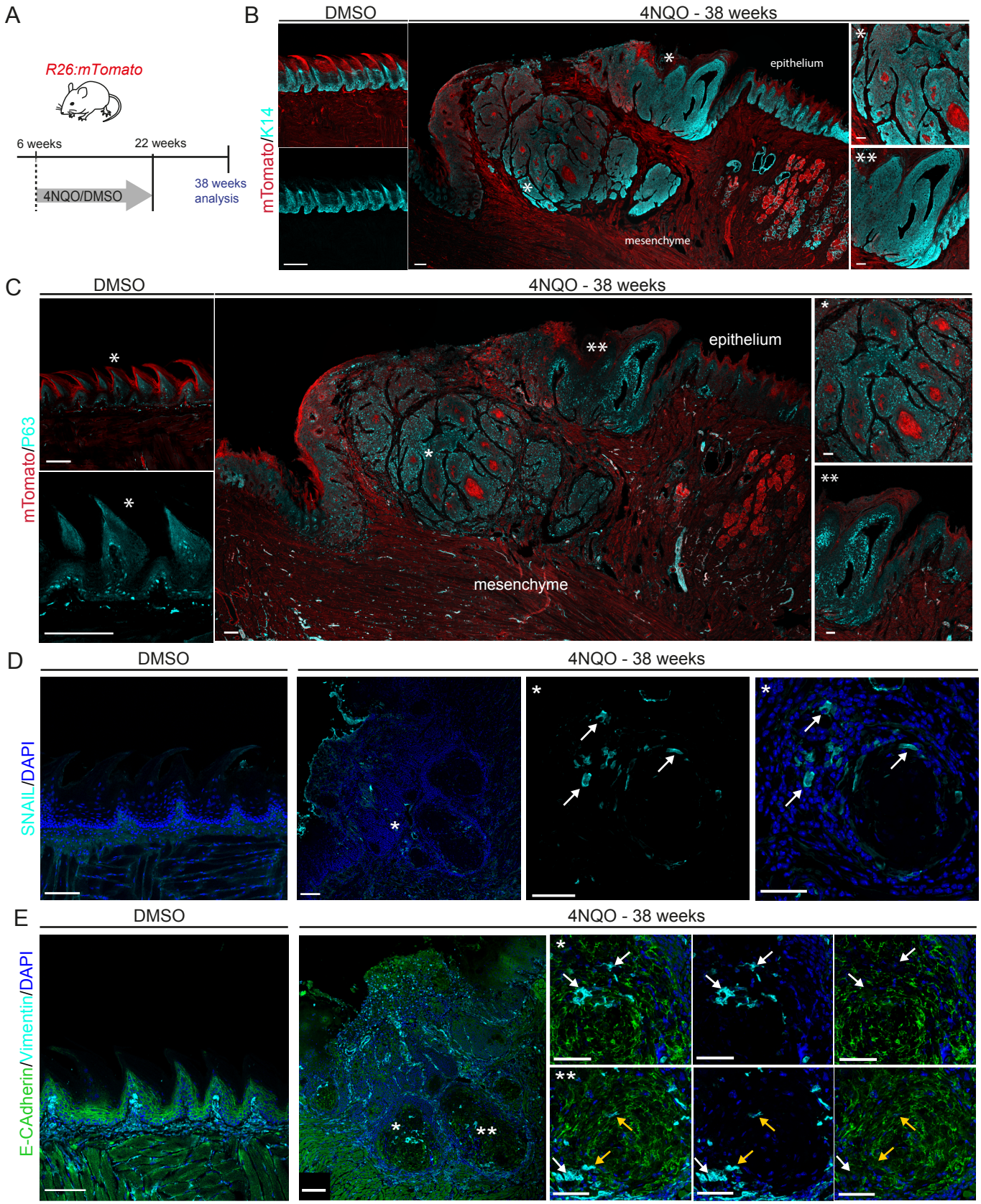

Figure 5: Notch1+ cells invade neighboring non-epithelial tissue

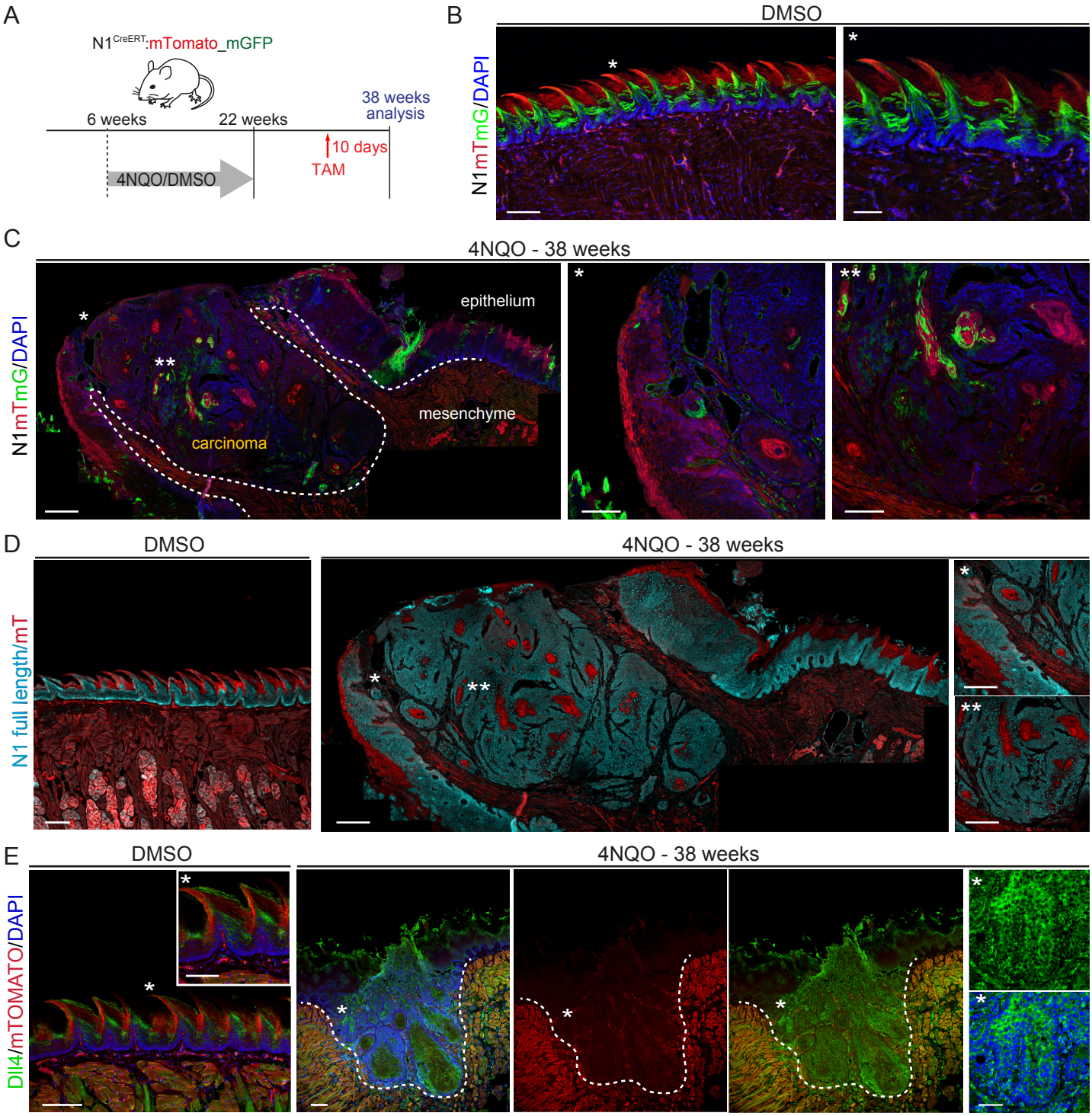

Figure 6: Transcriptome analyses of differentially expressed genes in cancerogenic versus control conditions

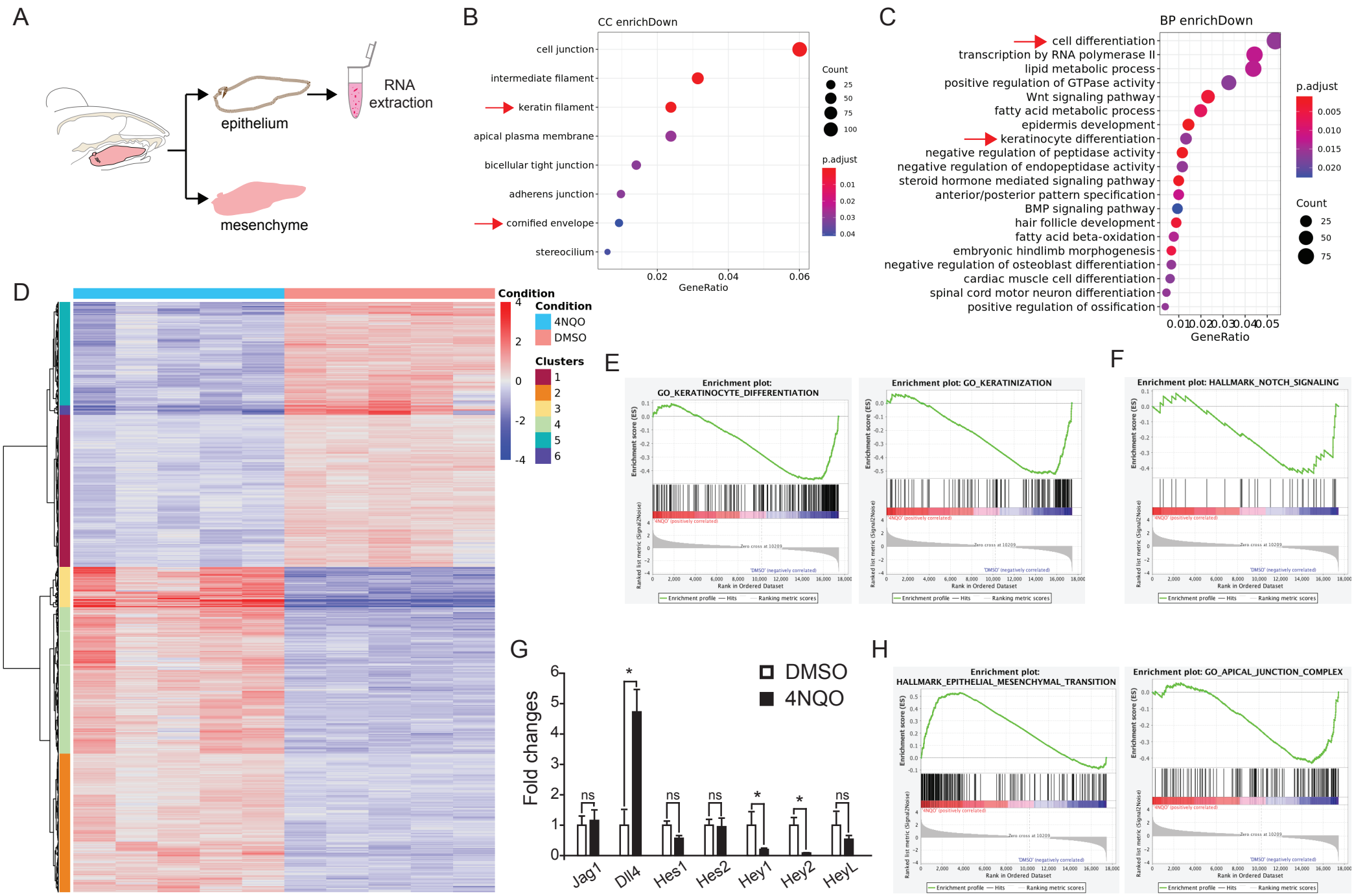
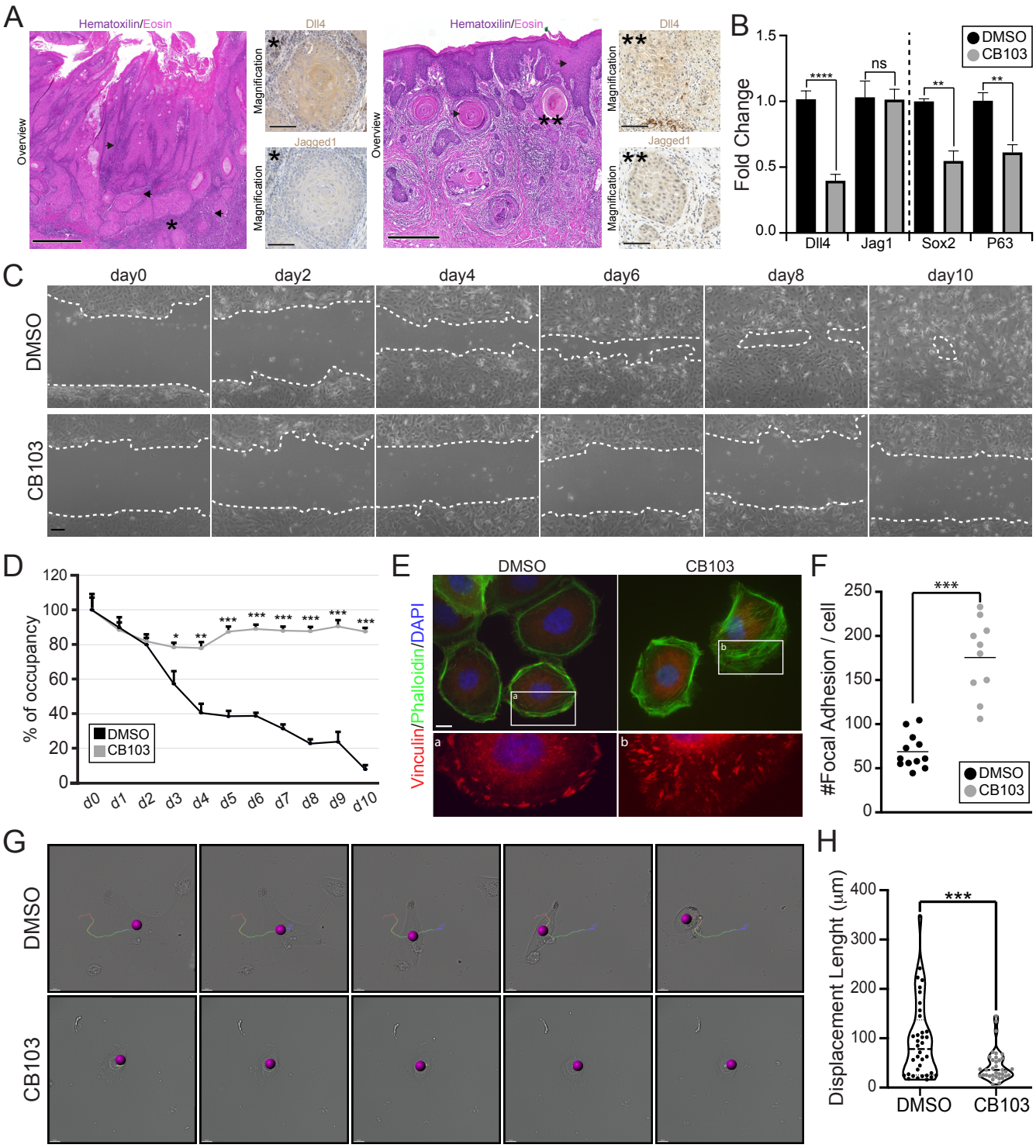
Figure 7: The Notch signaling pathway regulates malignancy in human squamous cell carcinoma